Disordered to ordered folding in the regulation of diphtheria toxin repressor activity

P. D. Twigg, G. Parthasarathy, L. Guerrero, T. M. Logan, and D. L. D. Caspar*

Institute of Molecular Biophysics, Florida State University, Tallahassee, FL 32306

Contributed by D. L. D. Caspar, July 10, 2001

Understanding how metal binding regulates the activity of the diphtheria toxin repressor protein (DtxR) requires information about the structure in solution. We have prepared a DtxR mutant construct with three additional N-terminal residues, Gly-Ser-His-DtxR(Cys-102 → Asp), that retains metal-binding capabilities, but remains monomeric in solution and does not bind DNA under conditions that effect dimerization and DNA binding in the functional DtxR(Cys-102 → Asp) construct. Although the interaction properties of this inactive mutant in solution are very different from that of active repressors, crystallization imposes the same dimeric structure as observed in all crystal forms of the active repressor with and without bound metal. Our solution NMR analyses of active and inactive metal-free diphtheria toxin repressors demonstrate that whereas the C-terminal one-third of the protein is well ordered, the N-terminal two-thirds exhibits conformational flexibility and exists as an ensemble of structural substates with undefined tertiary structure. Fluorescence binding assays with 1-anilino naphthalene-8-sulfonic acid (ANS) confirm that the highly α-helical N-terminal two-thirds of the apoprotein is molten globule-like in solution. Binding of divalent metal cations induces a substantial conformational reorganization to a more ordered state, as evidenced by changes in the NMR spectra and ANS binding. The evident disorder to order transition upon binding of metal in solution is in contrast to the minor conformational changes seen comparing apo- and holo-DtxR crystal structures. Disordered to ordered folding appears to be a general mechanism for regulating specific recognition in protein action and this mechanism provides a plausible explanation for how metal binding controls the DtxR repressor activity.

Diphtheria toxin repressor protein (DtxR) is a 226-amino acid residue, iron-dependent transcriptional regulator of genes in *Corynebacterium diphtheriae* that code for diphtheria toxin and proteins involved in iron uptake and oxidative stress (1, 2). DtxR is the best characterized member of a family of related proteins from primarily Gram-positive bacteria that regulate metal-sensitive genes (3). Activation of DtxR requires binding of Fe^{2+} or other divalent transition metal cations (4); the apoprotein is incapable of DNA binding, but the metal-activated dimer recognizes and binds to an interrupted palindromic DNA sequence in the promoter region (5). Whereas only one high-affinity metal-binding site per monomer was detected by binding assays (5, 6), the crystal structure of DtxR revealed the presence of two distinct metal-binding sites (7–9).

Purified DtxR readily forms disulfide-bridged dimers linked by the single cysteine residue at position 102, which Tao and Murphy (10) identified as a critical metal-binding ligand by using saturation site-directed mutagenesis. They demonstrated that Asp-102 could also function as a ligand for the metal, but substitution by all of the other 18 amino acids at this site produced inactive repressor. When the crystal structure of DtxR was determined (7, 8), the occupancies of Mn^{2+}, Fe^{2+}, Co^{2+}, Ni^{2+}, and Zn^{2+} detected at the Cys-102 site were negligible, but partial occupancy of this site by Cd^{2+} was observed (7). Oxidation of Cys-102 of the native DtxR under crystallizing conditions inhibited metal binding at this essential site for repressor activity. The crystal structure of the functional DtxR(Cys-102 → Asp) construct [DtxR(C102D)] showed full occupancy of Ni^{2+} at the essential metal-binding site with ligands Met-10, Asp-102, Glu-105, and His-106 (9).

Site-directed mutations of the other metal-binding site, formed by His-79, Glu-83, and His-98, indicated that it is not essential for metal dependent regulation (9); however, alanine substitutions for residues Arg-80, Ser-126, or Asn-130, which coordinate an anion linked to the metal in this site, decreased DtxR activity (11). The anion associated with the ancillary metal binding site [which was called site 1 because it was fully occupied in the first crystal structure of holo-DtxR (7)] may help to stabilize the dimer structure.

The N-terminal domain (residues 1–124) of DtxR contains the two separate metal binding sites, as well as a canonical prokaryotic helix–turn–helix DNA binding motif and the dimerization interface (7–9, 12–17). All of the analyzed DtxR crystals, with and without bound metal, have nearly identical dimeric N-terminal domain structures, but all have some degree of disorder in the C-terminal domain (residues 149–226), which is connected to the N-terminal domain by a flexible linker (7–9, 12–17). High-resolution data from a Co^{2+}-containing crystal revealed a Src homology 3 (SH3)-like fold for the C-terminal domain with a higher mean temperature factor than the N-terminal domain (12), but the crystallographic data could not distinguish whether this disorder was due to rigid body movement or internal fluctuations.

Solution NMR structural studies with the C-terminal construct DtxR(130–226) demonstrated that this domain folds independently of the N-terminal domain and is internally well ordered (18). Further NMR experiments showed that the SH3-like C-terminal construct binds a synthetic 15-aa peptide with the highly conserved sequence of the proline-rich segment (residues 125–139) linking the N- and C-terminal domains (19). Binding occurs in a manner similar to the specific binding of proline-containing peptides by eukaryotic SH3 domains. In solution, interaction of the DtxR C-terminal domain with the linker peptide of the metal-free repressor may function to inhibit dimerization and DNA recognition.

Because crystallization imposes essentially the same dimeric structure on the N-terminal domain of the aporepressor as that of the metal-activated dimer crystallized with or without DNA (7–9, 12–17), crystallography has provided no information about the structure of the inactive monomeric form of DtxR. To understand the dynamics involved in the switching mechanism of DtxR, we must look at the protein structure in solution. We have prepared a new DtxR construct, gsh-DtxR(C102D), with three additional residues at the N terminus (G.P., P.D.T., and D.L.D.C., unpublished data). The presence of the N-terminal

BIOPHYSICS

Abbreviations: DtxR, diphtheria toxin repressor protein; DtxR(C102D), functional Cys-102 → Asp mutant of DtxR; gsh-DtxR(C102D), nonfunctional mutant of DtxR(C102D) with Gly-Ser-His added at the N terminus; HSQC, heteronuclear single quantum correlation; ANS, 1-anilino naphthalene-8-sulfonic acid, ammonium salt; SH3, Src homology 3.

*To whom reprint requests should be addressed. E-mail: caspar@sb.fsu.edu.

The publication costs of this article were defrayed in part by page charge payment. This article must therefore be hereby marked "*advertisement*" in accordance with 18 U.S.C. §1734 solely to indicate this fact.

extension inhibits dimer formation in solution by gsh-DtxR(C102D) under conditions that generate dimer of DtxR and DtxR(C102D); moreover, there is no detectable binding of the mutant gsh-DtxR(C102D) to DNA in the presence of metal. Analysis of this mutant provides insights into the structure and dynamics of the N-terminal domain in the monomeric state.

What is the nature of the monomer structure, and what changes are effected by the metal-induced dimerization that facilitate recognition of the DNA operator sequence? We present evidence that the N-terminal domain of apo-DtxR is dynamically disordered in solution, in contrast with its highly ordered structure in metal-free crystals. The addition of divalent metal cations induces an ordering of the N-terminal domain structure, which indicates that, under physiological conditions, a disorder/order transition is involved in the regulation of DtxR activity.

Materials and Methods

Protein Expression and Purification. DtxR(C102D) was expressed in *Escherichia coli* HMS174(DE3)pET(C102D) (plasmid provided by Dr. John Murphy, Boston University Medical Center) as described (10). Cells were harvested by centrifugation and lysed by French press. Purification was by sequential passage over a DEAE-Sepharose anion-exchange column and a Ni^{2+} chelating column (Chelating Sepharose Fast Flow, Amersham Pharmacia).

The plasmid construct for gsh-DtxR(C102D) was generated by subcloning the DtxR(C102D) gene into pET-15b vector (Novagen) at the *Nde*I and *Bam*HI sites in the vector. This introduced a 6X-His tag and a thrombin cleavage site (to remove tag) at the N terminus of the protein. Expression in *E. coli* BL21(DE3) host cells was induced at OD_{600} of $\approx$0.5 with 1 mM isopropyl β-D-thiogalactoside (IPTG) for 2 h. Protein was purified by the procedure used for DtxR(C102D). The 6X-His tag was removed by digestion with thrombin (Novagen) for 16 h at 4°C, leaving three additional residues at the N terminus [Gly-Ser-His-DtxR(C102D)]. The final construct was purified over a benzamidine-Sepharose column (Amersham Pharmacia) to remove thrombin. With the exception of protein used in crystallization experiments, all protein samples were dialyzed against buffer containing 5 mM EDTA to remove trace amounts of Ni^{2+} leached from the Ni^{2+} chelating column.

Expression and purification of the C-terminal domain construct DtxR(130–226) was as described by Twigg *et al.* (18). A shorter C-terminal domain construct, DtxR(144–226), was expressed and purified as described by Wang *et al.* (19).

Uniformly ^{15}N-labeled samples of all proteins for use in NMR experiments were purified from cells grown in M9 minimal media containing 1 g/l $^{15}NH_4Cl$.

Gel Electrophoresis and Mobility Shift Assay. Nondenaturing PAGE was performed by using 12% gels. Samples of DtxR(C102D) and gsh-DtxR(C102D) were prepared at 10 μM protein in 10 mM Tris·HCl (pH 8.0) in the absence of $NiCl_2$, and at 4 μM protein in 10 mM Tris·HCl (pH 8.0) in the presence of 30 mM $NiCl_2$. Ni^{2+}-bound proteins were electrophoresed with gels and running buffers also made 30 mM $NiCl_2$. Proteins were stained with Coomassie brilliant blue.

The gel electrophoresis mobility-shift assay was similar to that described by Tao *et al.* (20). A 36-bp blunt-ended DNA probe containing the corynebacteriophage β *tox* operator sequence (*toxPO*) (20) was synthesized as two single-stranded oligonucleotides and the duplex formed by annealing. The dsDNA *toxPO* probe was labeled with [^{32}P]dATP by standard procedures (21). Binding of DtxR(C102D) and gsh-DtxR(C102D) protein at a concentration of 0.9 mM to the *toxPO* probe was assayed in 16 μl of reaction mixture containing 20 mM Tris·HCl (pH 7.5), 5 mM $MgCl_2$, 40 mM KCl, 2 mM DTT, 125 mM $MnCl_2$, 10% (vol/vol) glycerol, 1 μg of poly(dI-dC), 5 μg of BSA, and 3–5 fmol of ^{32}P-labeled *toxPO* probe. After addition of the probe, the reaction mixture was incubated for 15 min at 25°C and then analyzed by 6% polyacrylamide gel electrophoresis in 40 mM [bis(2-hydroxyethyl)amino]tris(hydroxymethyl)methane (Bis-tris) borate buffer (pH 7.5)/125 μM $MnCl_2$, at constant voltage (200 V). The gels were dried and analyzed by autoradiography.

Circular Dichroism Spectroscopy. Far-UV wavelength circular dichroism (CD) spectra of DtxR(C102D) and gsh-DtxR(C102D) were collected over a range from 280 nm to 190 nm with a 0.1-cm pathlength cuvette at 25°C by using an Aviv 62A spectropolarimeter. Samples of DtxR(C102D) and gsh-DtxR(C102D) were prepared in 50 mM sodium phosphate buffer (pH 7.0) at protein concentrations of 10 μM. Additional experiments were conducted with DtxR(C102D) in the presence and absence of $NiCl_2$ to examine the effects of metal binding on secondary structure. For this, samples of DtxR(C102D) were prepared at 4 μM concentration in 10 mM sodium phosphate buffer (pH 7.0) with and without the addition of 20 μM $NiCl_2$ and spectra collected as above.

X-Ray Crystallography. Crystals of gsh-DtxR(C102D) were obtained by the hanging drop method under conditions similar to those reported for DtxR (8). Ten-microliter drops of 9 mg/ml protein/50 mM sodium phosphate (pH 8–8.5)/1.4–1.5 M ammonium sulfate were equilibrated against 1-ml reservoirs of 50 mM sodium phosphate (pH 8–8.5)/2.8–3.0 M ammonium sulfate at room temperature. Protein samples used for crystallization were not treated with EDTA after purification with the Ni^{2+} affinity column. Crystals grew over a period of 1–2 weeks. Data were collected at 4°C on a Rigaku RU-200 rotating anode generator fitted with an R-Axis II imaging plate detector. Data processing was performed by using DENZO (22) and CCP4 (23) software.

NMR Studies. NMR spectra were acquired on either a 500 MHz or 720 MHz three-channel Varian Unity*plus* instrument equipped with waveform generators and pulsed field gradient accessories. The two-dimensional ^1H, ^{15}N-heteronuclear single quantum correlation (HSQC) spectra (24) were collected on the 500-MHz instrument with sweep widths of 8333.33 Hz and 512 complex points and 1650 Hz and 140 complex points in the ^1H (ω2) and ^{15}N (ω1) dimensions, respectively; and on the 720-MHz instrument with sweep widths of 12,001.20 Hz and 512 complex points and 2500 Hz and 140 complex points in the ^1H (ω2) and ^{15}N (ω1) dimensions, respectively. Samples of DtxR(C102D) and gsh-DtxR(C102D) were prepared at 1 mM protein concentration in 10 mM sodium phosphate buffer (pH 7.0). DtxR(130–226) and DtxR(144–226) were prepared at 1 mM protein concentration in 10 mM potassium phosphate buffer (pH 7.5). Samples of metal-bound DtxR(C102D) were prepared by addition of 100 mM $CdCl_2$ stock to a final concentration of 2 mM $CdCl_2$ in 0.5 mM protein/10 mM sodium phosphate buffer (pH 7.0). Samples of metal-bound gsh-DtxR(C102D) were prepared with 3 mM $CdCl_2$/1 mM protein/10 mM sodium phosphate buffer (pH 7.0).

ANS Binding Fluorescence Assays. Samples of DtxR(C102D), gsh-DtxR(C102D), and DtxR(130–226) were prepared with 500 μM 1-anilino naphthalene-8-sulfonic acid (ANS)/5 μM protein in 50 mM sodium phosphate buffer (pH 7.0). Emission spectra were collected at 25°C over a range from 380–600 nm with an excitation wavelength of 365 nm (25, 26) by using a Perkin–Elmer LS-50 fluorescence spectrometer. Samples of protein prepared with $CoCl_2$ were first mixed with 5:1 molar ratio $CoCl_2$:protein in a stock solution (0.8 mM $CoCl_2$/0.16 mM protein), incubated at 25°C for 15 min, then diluted to 5 μM protein/500 μM ANS/1 mM $CoCl_2$/50 mM sodium phosphate (pH 7.0).

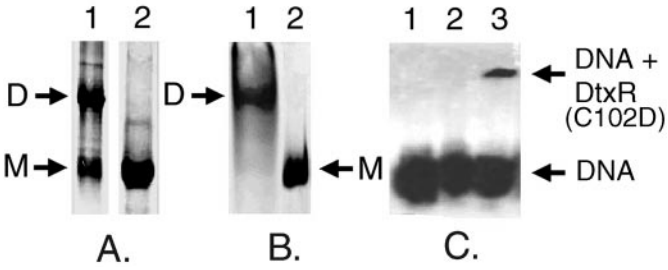

Fig. 1. Gel electrophoresis. (*A*) A composite 12% nondenaturing polyacrylamide gel; 10 μM protein in the absence of metal. Lane 1 [DtxR(C102D)] shows bands for both monomer and dimer, whereas lane 2 [gsh-DtxR(C102D)] has a single monomer band. The minor band in lane 2 at a molecular weight of 43 kDa is a contaminant present in incompletely purified repressor samples. (*B*) A composite 12% nondenaturing polyacrylamide gel; 4 μM protein in the presence of 30 mM $NiCl_2$. Lane 1 [DtxR(C102D)] shows a single dimer band, whereas lane 2 [gsh-DtxR(C102D)] shows a single monomer band. (*C*) Gel mobility-shift assay. Lane 1 is *toxPO* probe alone, lane 2 is gsh-DtxR(C102D) + *toxPO* probe, and lane 3 is DtxR(C102D) + *toxPO* probe. Only DtxR(C102D) shows binding to *toxPO* DNA.

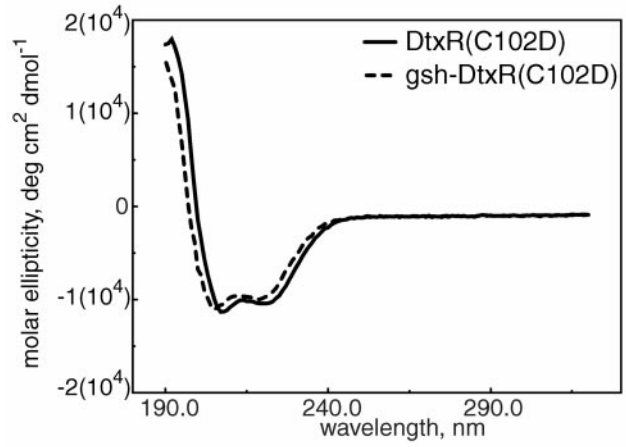

Fig. 2. Far-UV circular dichroism spectra for DtxR(C102D) and gsh-DtxR(C102D). The nearly coincident spectra of DtxR(C102D) (solid line) and gsh-DtxR(C102D) (dashed line) indicate similar predominantly α-helical secondary structure.

Results

Comparison of Repressor With and Without N-Terminal Extension. *Gel electrophoresis.* Nondenaturing polyacrylamide gels run with metal-free protein samples at 10 μM protein concentration indicated that gsh-DtxR(C102D) showed no evidence of dimerization, whereas DtxR(C102D) had a significant dimer component (Fig. 1*A*). To determine whether divalent metal cations could induce dimerization in gsh-DtxR(C102D), samples of gsh-DtxR(C102D) and DtxR(C102D) at 4 μM concentration were incubated with saturating amounts of Ni^{2+} (30 mM) and electrophoresed on native gels. Metal-binding resulted in essentially complete dimerization of DtxR(C102D), but had no apparent effect on gsh-DtxR(C102D) (Fig. 1*B*), although assays of metal-binding by fluorescence spectroscopy show that metal is bound by gsh-DtxR(C102D) with affinity similar to that of DtxR(C102D) (G.P., P.D.T., and D.L.D.C., unpublished data). The inability of metal to induce dimerization in gsh-DtxR(C102D) at 4 μM protein implied that DNA-binding activity would also be impaired, and this was confirmed by gel mobility-shift assays (Fig. 1*C*). This assay, which demonstrates binding of metal-activated DtxR(C102D) to the DNA probe containing the corynebacteriophage β encoded *tox* operator sequence, failed to show any interaction between gsh-DtxR(C102D) and DNA under the same experimental conditions.

Circular dichroism. Circular dichroism (CD) spectra demonstrated that the secondary structure of gsh-DtxR(C102D) and DtxR(C102D) in solution were very similar (Fig. 2). Spectral minima occurring at 208 nm and 222 nm, which dominate the spectra, are characteristic of α-helices (27). A slight shift in the overall spectrum to lower wavelengths for gsh-DtxR(C102D) might indicate some minor change in the secondary structure as compared with DtxR(C102D). The spectra of both DtxR(C102D) and gsh-DtxR(C102D) were consistent with a predominant α-helical conformation, as observed in the crystalline state, and the three additional residues in gsh-DtxR(C102D) did not result in significant changes to the α-helical content. The CD spectrum of DtxR(C102D) bound to Ni^{2+} was identical with that of apo-DtxR(C102D) (data not shown) indicating that whatever conformational changes may occur on metal binding, they do not result in a detectable change in secondary structure.

Crystal structure of gsh-DtxR(C102D). X-ray diffraction data collected at 4°C with a 0.4 × 0.3 × 0.3 mm gsh-DtxR(C102D) crystal were 97% complete to 2.3 Å resolution with an R_{symm} of 0.05. The space group was $P3_121$ with unit cell dimensions a = b = 63.9 Å, c = 109.6 Å, and one monomer in the asymmetric unit. These crystallographic parameters are close to those reported for previous DtxR structures, whose a = b axes range from 63.2–64.9 Å and c axes from 105.5–109.3 Å (7, 8, 12, 15). An initial $2F_o$-F_c electron density map was generated with ARP/wARP 5.1 (28), using phases calculated from a 137-residue model for the N-terminal domain taken from the Protein Data Bank entry 2dtr (12), whose cell dimensions a = b = 63.9 Å and c = 109.3 Å are nearly the same as the gsh-DtxR(C102D) crystal. This is the structure of a wild-type DtxR complexed with Co^{2+}, but the metal and associated sulfate ion at "site 1" were omitted from the model. The initial protein model was replaced by a free atom model created for subsequent rounds of refinement.

Our refined electron density map revealed that the overall structure of gsh-DtxR(C102D) is very similar to all of the dimeric DtxR and DtxR(C102D) structures reported to date (7–9, 12–17). We noted the presence of strong electron density in the anion binding site and in both metal binding sites, although no metal was added in crystallization or in the starting atomic model. The bound metal may be Ni^{2+} ions which have leached from the Ni^{2+} affinity column in purification or Fe^{2+} ions present in the growth medium. Fig. 3 shows a portion of the electron density map at the dimer interface, including the well ordered Trp-104 and Leu-85, whose density closely fits the reference atomic model 2dtr (12). The comparison between the reference model near the N terminus (residues Leu-4 and Val-5) and the refined density map indicates a different structure in the N-terminal portion of gsh-DtxR(C102D). The three additional residues at the N terminus of gsh-DtxR(C102D) evidently perturb this part of the structure, which is disordered for at least the first two or three residues in other crystals of DtxR and DtxR(C102D) (7–9, 12–17). Despite gel electrophoresis data demonstrating lack of any dimer formation in solution at protein concentrations of 10 μM in the absence of Ni^{2+} ions and 4 μM in its presence (Fig. 1), gsh-DtxR(C102D) crystallizes in the normal dimer form (Fig. 3). This implies that under crystallization conditions of 0.72 mM protein and 2.8–3.0 M ammonium sulfate, the monomer/dimer equilibrium is forced to the dimer state.

Repressor N-Terminal Domain Structure in Solution. *Two-dimensional ^1H,^{15}N HSQC NMR spectra.* Two-dimensional ^1H,^{15}N correlation spectra (24) were collected on uniformly ^{15}N-labeled

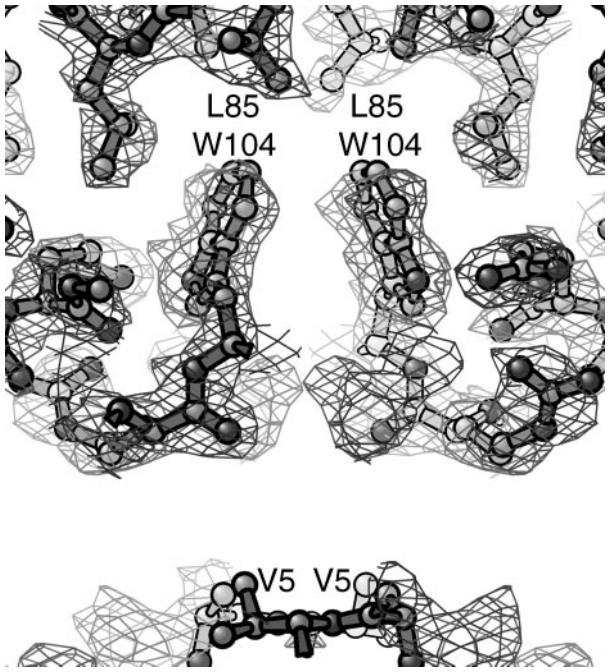

Fig. 3. Electron density map of the gsh-DtxR(C102D) structure at the dimer interface, compared with a DtxR model. This 7.5-Å slab of the 2.3-Å resolution $2F_o$-F_c map, contoured at 1.2 σ, is viewed perpendicular to the crystallographic 2-fold axis. The map is overlaid with a model structure for DtxR taken from Protein Data Bank coordinates (PDB ID code 2dtr) to illustrate the strong similarities between the two protein structures. There is electron density present at the N terminus that does not fit with the overlaid model and may indicate some local conformational differences. The figure was generated by using BOBSCRIPT, an enhanced version of MOLSCRIPT (44).

DtxR(C102D) and gsh-DtxR(C102D) at 30°C (Fig. 4*A* and Figs. 6 and 7, which are published as supporting information on the PNAS web site, www.pnas.org). The vast majority of the observed DtxR(C102D) resonances (Fig. 4*A*, cyan peaks) could immediately be assigned to the C-terminal domain by their overlap with the spectrum for DtxR(130–226) (Fig. 4*A*, orange peaks; refs. 18 and 19). Only a few additional resonances were possibly attributable to the N-terminal domain. A number of the C-terminal domain resonances exhibit slight shifts in the DtxR(C102D) and gsh-DtxR(C102D) constructs compared with DtxR(130–226), indicating some subtle changes in the chemical environment of the backbone amide nitrogen and/or proton atoms. It is evident that the C-terminal domain is folded in both the full-length proteins in a SH3-like structure very similar to that seen in the C-terminal domain constructs (19). Two resonances assigned to Gly-134 and Gly-139, which are located in the flexible linker region, have disappeared in the full-length protein, either because of broadening or substantial changes in chemical shift values. Four additional peaks clustered near the random coil region (Fig. 4*A Inset*) may be due to splitting of C-terminal domain resonances, or may arise from N-terminal domain amino acids. Other than these, there are no resonances in the spectra of DtxR(C102D) and gsh-DtxR(C102D) at 30°C (see Fig. 6), which can be attributed to any of the 124 amino acids in the N-terminal domain.

Gel mobility assays and rigorous removal of contaminating metal showed that proteolytic degradation or paramagnetic metal ion binding were not the source of the missing N-terminal resonances (data not shown). The most plausible explanation for the invisibility of almost all of the N-terminal domain in the NMR spectrum at 30°C is exchange among different conformational substates on an intermediate time scale. If the differences in resonance frequencies of these substates are comparable to their exchange rates, these resonances would be broadened beyond detection.

To alter the exchange rates, HSQC spectra were collected from the metal-free protein at 4°C, resulting in the appearance of additional resonances that must be from the N-terminal domain (Fig. 4*B*, cyan peaks, and Figs. 8–11, which are published as supporting information on the PNAS web site). Of these new resonances, two classes can be identified. Well resolved resonances (from ≈7.9 to ≈8.5 ppm in the ^{1}H dimension, and ≈123 to ≈133 ppm in the ^{15}N dimension), with narrow line widths and low chemical-shift dispersion, are consistent with some ordered structure in the N-terminal domain (Fig. 4*B*, Box 1). Diffuse, broadened resonances in the random-coil region (from ≈8.2 to ≈8.7 ppm in the ^{1}H dimension) represent more flexible portions of the structure (Fig. 4*B*, Box 2). The broadened resonances for the disordered regions of DtxR(C102D) and gsh-DtxR(C102D) were in contrast to the narrow line widths seen in a spectrum of gsh-DtxR(C102D) unfolded with 8 M urea (see Fig. 12, which is published as supporting information on the PNAS web site). This comparison demonstrates that the metal-free repressor is not randomly unfolded, but appears to be fluctuating among different conformations on the intermediate time scale. Fluctuations among discrete conformations were also evident from the presence of multiple resonances in the region associated with the NH of the unique tryptophan residue side chain (Trp-104; Fig. 4*B*, Box 3), which forms part of the dimer interface (Fig. 3). At the 1 mM concentration of apo-DtxR(C102D) used for the NMR experiments, extensive dimer formation is likely, because nondenaturing gels showed significant dimerization at 100-fold lower concentrations (Fig. 1*A*). Thus, the disorder detected by NMR spectroscopy may indicate fluctuating dimer structures.

Stabilizing active dimer by adding Cd^{2+} [a nonparamagnetic cation that binds at both metal sites in DtxR (8)] resulted in substantial changes in the NMR spectrum of DtxR(C102D) at 4°C (Fig. 4*B*, red peaks). In particular, we observed additional well defined peaks in the ordered region (Box 1) and a disappearance or sharpening of many resonances found in the central region (Box 2). There is a downfield shift in the Trp-104 side chain NH resonance (Box 3) with multiple resonances still observed, indicating that the metal-activated dimeric structure is not yet uniquely ordered in solution. Adding Cd^{2+} to gsh-DtxR(C102D) resulted in a similar sharpening of resonances, but not as extensively as with DtxR(C102D) (see Fig. 8).

ANS fluorescence binding assays for molten globule state. Our NMR data together with circular dichroism (CD) data suggest that the predominantly α-helical N-terminal domain of the repressor adopts a molten globule-like structure (29) in the absence of metal. ANS binds to exposed hydrophobic surfaces, such as those found in molten globules (25, 26), and may be used to probe the accessibility of the protein interior. When bound to a susceptible protein, the intrinsic fluorescence of ANS is substantially increased. As seen in Fig. 5, ANS interacts strongly with both DtxR(C102D) and gsh-DtxR(C102D), providing evidence for a loose, internally-accessible structure in solution. The interaction of ANS was specific for the N-terminal domain, because ANS does not bind to the C-terminal domain construct DtxR(130–226) (Fig. 5*A*). When Co^{2+} was added, the binding of ANS to DtxR(C102D) (Fig. 5*A*) and gsh-DtxR(C102D) (Fig. 5*B*) was significantly reduced, as indicated by the diminished fluorescence. This diminished ANS binding is consistent with the NMR observations, which demonstrate a more ordered structure for the N-terminal domain in the presence of metal.

Discussion

Weber (30) recognized that the nature of protein molecules in solution is more dynamic than x-ray crystallographic structures would suggest: rather than occupying a single well ordered

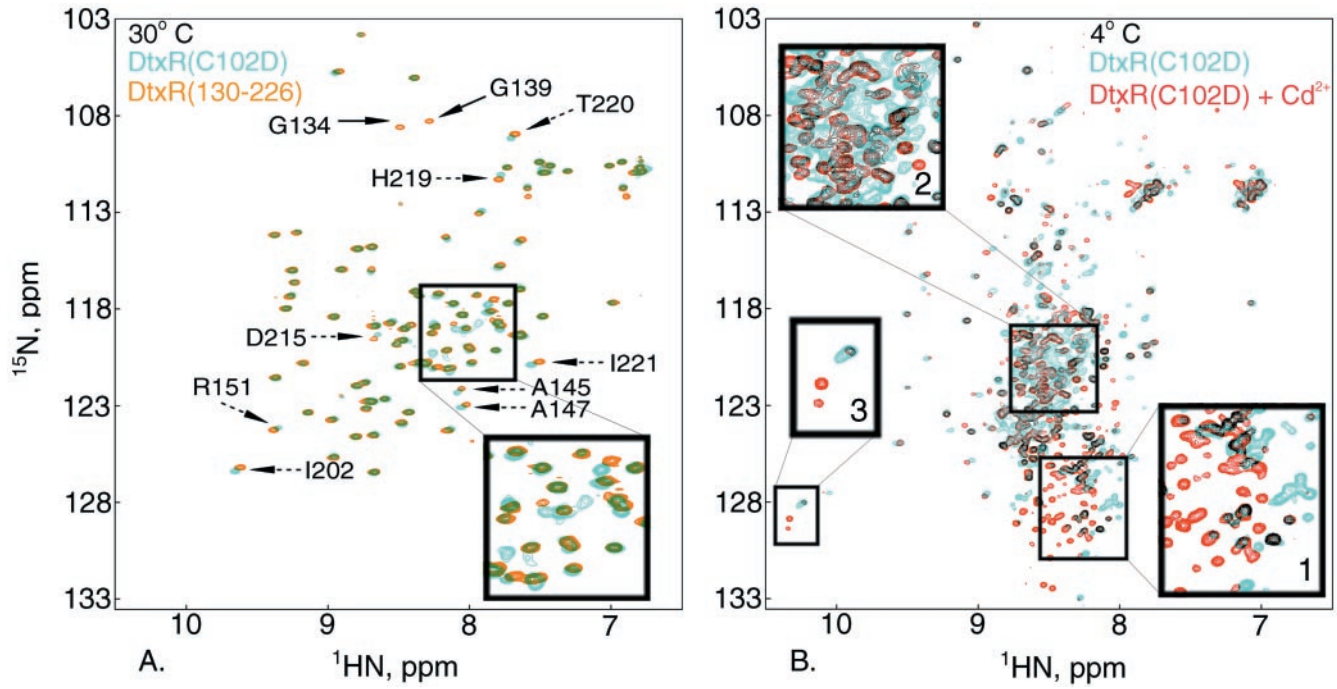

Fig. 4. (*A*) Overlay of two-dimensional ^{1}H,^{15}N-HSQC spectra comparing 1 mM full-length DtxR(C102D) (cyan) with 1 mM DtxR(130–226) C-terminal domain construct (orange) at 30°C. Overlapping areas are green. The resonances present for the full-length protein are primarily assignable to the C-terminal domain. A number of the C-terminal domain resonances (dashed arrows) exhibit slight shifts in the full-length constructs compared with DtxR(130–226), indicating some subtle changes in the SH3-like fold in these two structures. Two linker region resonances (solid arrows) have disappeared in the full-length protein. The box indicates a region of the spectrum with a small number of additional resonances that may be attributable to the N-terminal domain. (*B*) Comparison of 1 mM DtxR(C102D) in the absence (cyan) and 0.5 mM DtxR(C102D) in the presence (red) of 2 mM $CdCl_2$ at 4°C. Overlapping areas are black. Box 1 indicates peaks that have narrow line widths and upfield-shifted ^{1}H resonances consistent with ordered structure. The number of resonances in this box increases with the addition of metal. Box 2 highlights the broadened resonances present in the random coil region of the spectrum characteristic of more disordered regions of the structure in intermediate exchange, and shows the disappearance of some resonances and sharpening of others in the presence of metal. Box 3 contains the resonances tentatively assigned to the single Trp-104 side chain NH. Note that there are multiple peaks both in the absence and presence of metal, indicating more than one conformation is present at this site.

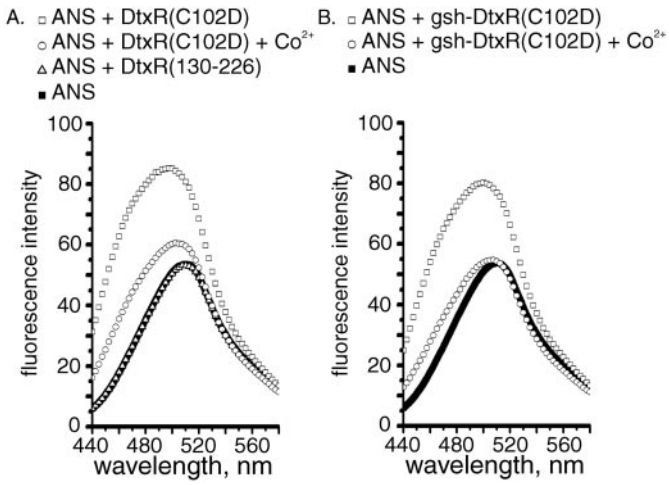

Fig. 5. (*A*) ANS fluorescence spectra in the presence of DtxR(C102D) and C-terminal domain construct DtxR(130–226). A significant increase in fluorescence is detected on binding of ANS to DtxR(C102D). This fluorescence is substantially diminished in the presence of $CoCl_2$, which indicates an ordering of the N-terminal domain of the DtxR(C102D) structure when metal is bound. The assay with DtxR(130–226) confirms that ANS does not bind the SH3-like C-terminal domain. (*B*) ANS fluorescence spectra in the presence of gsh-DtxR(C102D), with and without the addition of $CoCl_2$, show results similar to that seen with DtxR(C102D). ANS spectra alone are repeated in both plots for reference.

conformation, a protein in solution may be a "kicking and screaming stochastic molecule" sampling a number of conformational substates. Increasing numbers of proteins have been identified as having loops or complete domains that are intrinsically unstructured (i.e., lacking a well defined tertiary structure) under physiological conditions. Many of these loose structures participate in DNA recognition and transcriptional activation (31–35), or in protein self-assembly (36, 37). This lack of ordered structure may provide the protein with the ability to adapt to and recognize different target molecules or may enhance an inducible response to changing environmental conditions. In many cases the trigger for folding may be binding to a target molecule or ligand (38).

From analysis of the NMR spectra and ANS binding assays, we have demonstrated that the N-terminal domain of apo-DtxR adopts a loosely folded structure in solution. Evidence for metal-induced ordering comes from the decreased affinity of ANS for the interior of the N-terminal domain in the presence of Co^{2+} and from the Cd^{2+}-induced changes in the NMR spectra. Although crystallographic reports (7, 8, 15–17) have referred to the N-terminal region as being separated into a DNA-binding and a dimerization domain, we see no distinct separation in conformational behavior between these two segments and therefore classify the N-terminal domain as the entire loosely ordered part of the apo-DtxR structure (residues 1–124).

A puzzling observation that was unexplained until now is that, under oxidizing conditions, DtxR forms inactive disulfide-bridged dimers that can be converted to active repressor by the addition of a reducing agent (5). The distance between the two

BIOPHYSICS

Cys-102 S^{γ} atoms that form the disulfide bond is ≈23 Å in the crystalline dimer (7–9, 12–17). Rigid-body docking experiments by Qiu *et al.* (7) showed a disulfide-linked dimer could not be formed with the conformation of monomers as seen in the crystal structure without a significant rearrangement of the helices containing these residues. The substantial conformational fluctuations of the N-terminal domain we report here can account for the formation of a disulfide bridge.

Crystallographic studies of DtxR and DtxR(C102D) have been used to infer roles for the two metal-binding sites in altering the structure of the N-terminal domain to enhance DNA binding (7–9, 12–17). It is difficult to imagine that the limited differences between apo- and holo-repressor structures in the crystals can account for the significant functional differences between the apo and holo forms. Cocrystals of metal-bound dimer complexed with DNA (14, 16) provide a picture of how dimer binds to DNA, but without information about the structure of the metal-free protein in solution, the nature of control mechanisms involved in DNA recognition are obscure. Our evidence that a disorder to order folding transition takes place on binding to metal can account for the increase in dimer stability and DNA affinity.

The crystal structure of gsh-DtxR(C102D), which is innately monomeric in solution, is well enough resolved to establish that the dimeric structure (Fig. 3) is not significantly different from that in crystals of functional repressor (7–9, 12–17). Furthermore, Pohl *et al.* (17) have recently reported the crystallization of three inactive DtxR mutants with essentially the same dimeric structure as native DtxR. Because crystallization locks in the ordered dimeric structure, even with inactive mutants, caution should be used in inferring metal-activation mechanisms on the basis of the minor structural changes observed between crystals of apo- and holo-repressors.

DtxR acts as a global regulator of multiple genes involved in iron uptake, toxicity, and oxidative stress. No fewer than six different genes in *Corynebacterium diphtheriae* in addition to corynephage β *tox* have been identified as transcriptionally regulated by DtxR (39–41). This would suggest that some adaptability in DNA recognition may be necessary. In solution an equilibrium exists between apomonomer and apodimer of DtxR, and neither form is capable of binding DNA (42). We propose that the apoprotein exists as a highly flexible family of structural substates, even in the metal-free dimeric form, which becomes more ordered on binding transition metal cations. Although it is likely that all the DtxR crystal structures are representative of the active dimeric state, evidence from our NMR spectra and ANS binding experiments reveals that there are large structural fluctuations in solution that were not previously anticipated.

The biotin repressor BirA, the activity of which is controlled by binding the adenylate of biotin (43), has many properties in common with DtxR. In contrast to the crystallographic analysis of apo- and holo-DtxR, comparison of the monomeric apo-BirA crystal structure with that of the holo-BirA/biotin dimer has provided direct evidence for ordering of loops in the dimer interface that are disordered in the apomonomer (35). Disorder to order folding transitions in DtxR and BirA are key elements in the regulation of their repressor activities and provide important answers to the question of how their allosteric effectors modulate dimerization and DNA binding affinity.

We thank Dr. John Murphy of Boston University Medical center for the gift of a DtxR(C102D) plasmid. This work was supported by Research Training Grant NSF95114 from the National Science Foundation (to P.D.T.), U.S. Public Health Service research grants from the National Institute of General Medicine (GM54035 to T.M.L.) and National Cancer Institute (CA 47439 to D.L.D.C.), and by the National High Magnetic Field Laboratory.

1. Boyd, J., Oza, M. & Murphy, J. R. (1990) *Proc. Natl. Acad. Sci. USA* **87,** 5968–5972.
2. Schmitt, M. P. & Holmes, R. K. (1991) *Infect. Immun.* **59,** 1899–1904.
3. Holmes, R. K. (2000) *J. Infect. Dis.* **181,** S156–S167.
4. Tao, X. & Murphy, J. R. (1992) *J. Biol. Chem.* **267,** 21761–21764.
5. Tao, X., Zeng, H.-Y. & Murphy, J. R. (1995) *Proc. Natl. Acad. Sci. USA* **92,** 6803–6807.
6. Wang, Z., Schmitt, M. P. & Holmes, R. K. (1994) *Infect. Immun.* **62,** 1600–1608.
7. Qiu, X., Verlinde, C. L. M. J., Zhang, S., Schmitt, M. P., Holmes, R. K. & Hol, W. G. J. (1995) *Structure* **3,** 87–100.
8. Schiering, N., Tao, X., Zeng, H., Murphy, J. R., Petsko, G. A. & Ringe, D. (1995) *Proc. Natl. Acad. Sci. USA* **92,** 9843–9850.
9. Ding, X., Zeng, H., Schiering, N., Ringe, D. & Murphy, J. R. (1996) *Nat. Struct. Biol.* **3,** 382–387.
10. Tao, X. & Murphy, J. R. (1993) *Proc. Natl. Acad. Sci. USA* **90,** 8524–8528.
11. Goranson-Siekierke, J., Pohl, E., Hol, W. G. J. & Holmes, R. K. (1999) *Infect. Immun.* **67,** 1806–1811.
12. Qiu, X., Pohl, E., Holmes, R. K. & Hol, W. G. J. (1996) *Biochemistry* **35,** 12292–12302.
13. Pohl, E., Qiu, X., Must, L. M., Holmes, R. K. & Hol, W. G. J. (1997) *Protein Sci.* **6,** 1114–1118.
14. White, A., Ding, X., vanderSpek, J. C., Murphy, J. R. & Ringe, D. (1998) *Nature (London)* **394,** 502–506.
15. Pohl, E., Holmes, R. K. & Hol, W. G. J. (1998) *J. Biol. Chem.* **273,** 22420–22427.
16. Pohl, E., Holmes, R. K. & Hol, W. G. J. (1999) *J. Mol. Biol.* **292,** 653–667.
17. Pohl, E., Goransen-Siekierke, J., Choi, M. K., Roosild, T., Holmes, R. K. & Hol, W. G. J. (2001) *Acta Crystallogr. D* **57,** 619–627.
18. Twigg, P. D., Wylie, G. P., Wang, G., Caspar, D. L. D., Murphy, J. R. & Logan, T. M. (1999) *J. Biomol. NMR* **13,** 197–198.
19. Wang, G., Wylie, G. P., Twigg, P. D., Caspar, D. L. D., Murphy, J. R. & Logan, T. M. (1999) *Proc. Natl. Acad. Sci. USA* **96,** 6119–6124.
20. Tao, X., Boyd, J. & Murphy, J. R. (1992) *Proc. Natl. Acad. Sci. USA* **89,** 5897–5901.
21. Sambrook, J., Fritsch, E. F. & Maniatis, T., eds. (1989) Molecular Cloning: A Laboratory Manual (Cold Spring Harbor Lab. Press, Plainview, New York), 2nd Ed.
22. Otwinowski, Z. & Minor, W. (1997) *Methods Enzymol.* **276,** 307–326.
23. Collaborative Computational Project, Number 4 (1994) *Acta Crystallogr. D* **50,** 760–763.
24. Kay, L. E., Keifer, P. & Saarinen, T. (1992) *J. Am. Chem. Soc.* **114,** 10663–10665.
25. Semisotnov, G. V., Rodionova, N. A., Razgulyaev, O. I., Uversky, V. N., Gripas, A. F. & Gilmanshin, R. I. (1991) *Biopolymers* **31,** 119–128.
26. Ptitsyn, O. B. (1992) in *Protein Folding*, Creighton, T. E., ed. (Freeman, New York), pp. 243–299.
27. Adler, A. J., Greenfield, N. J. & Fasman, G. D. (1973) *Methods Enzymol.* **27,** 675–735.
28. Perrakis, A., Morris, R. J. & Lamzin, V. S. (1999) *Nat. Struct. Biol.* **6,** 458–463.
29. Ohghusi, M. & Wada, A. (1983) *FEBS Lett.* **164,** 21–24.
30. Weber, G. (1975) *Adv. Protein Chem.* **29,** 1–83.
31. Spolar, R. S. & Record, M. T., Jr. (1994) *Science* **363,** 777–784.
32. Wright, P. E. & Dyson, H. J. (2000) *J. Mol. Biol.* **293,** 321–331.
33. Daughdrill, G. W., Hanely, L. J. & Dahlquist, F. W. (1998) *Biochemistry* **37,** 1076–1082.
34. Kohler, J. J., Metallo, S. J., Schneider, T. L. & Schepartz, A. (1999) *Proc. Natl. Acad. Sci. USA* **96,** 11735–11739.
35. Weaver, L. H., Kwon, K., Beckett, D. & Matthews, B. W. (2001) *Proc. Natl. Acad. Sci. USA* **98,** 6045–6050.
36. Caspar, D. L. D. (1991) *Curr. Biol.* **1,** 30–32.
37. Namba, K. (2001) *Genes Cells* **6,** 1–12.
38. Parker, D., Rivera, M., Zor, T., Henrion-Caude, A., Radhakrishnan, I., Kumar, A., Shapiro, L. H., Wright, P. E., Montminy, M. & Brindle, P. K. (1999) *Mol. Cell. Biol.* **19,** 5601–5607.
39. Schmitt, M. P. & Holmes, R. K. (1994) *J. Bacteriol.* **176,** 1141–1149.
40. Lee, J. H., Wang, T., Ault, K., Liu, J., Schmitt, M. P. & Holmes, R. K. (1997) *Infect. Immun.* **65,** 4273–4280.
41. Schmitt, M. P. (1997) *Infect. Immun.* **65,** 4634–4641.
42. Lee, J. H. & Holmes, R. K. (2000) *J. Bacteriol.* **182,** 432–438.
43. Abbott, J. & Beckett, D. (1993) *Biochemistry* **32,** 9649–9656.
44. Kraulis, P. (1991) *J. Appl. Crystallogr.* **24,** 946–950.